TURBULENT INVERSION AND ENTRAINMENT INTO STRATOCUMULUS TOPPED BOUNDARY LAYER

Szymon P. Malinowski[1], Marta K. Kopeć[1], Wojciech Kumala[1], Katarzyna Nurowska[1]
Hermann Gerber[2], DjamalKhelif[3]

[1]University of Warsaw, Faculty of Physics, Institute of Geophysics, Pasteura 7, 02-093 Warsaw, Poland
[2]Gerber Scientific Inc., Reston, VA, USA.
[3]Department of Mechanical & Aerospace Engineering and Earth System Science, University of California Irvine, CA, USA.

1. INTRODUCTION

Exchange processes between stratocumulus and free troposphere above have been intensively investigated in many research campaigns (see e.g. Albrecht et al. (1988), Lenshow et. al. (1988), Stevens et al. (2003), Bretherton et al. (2004)). Despite the fact that marine stratocumulus is a relatively simple system: almost plain-parallel, warm cloud occupying the upper part of the well mixed boundary layer above a homogeneous flat surface, understanding entrainment into the stratocumulus topped boundary layer (STBL) is limited. Consequently, estimates of the entrainment velocity are ambiguous (e.g. Stevens (2002), Gerber et al. (2005), Faloona et al. (2005), Lilly (2008)). Data from in-situ measurements (e.g. Caughley et al. (1982), Nicholls (1989), Lenshow et. al. (2000), Rode and Wang (2007)) and results of numerical simulations (e.g. Moeng et.al. (2005), Yamaguchi and Randall (2008)) clearly indicate that top of the stratocumulus is located below the capping inversion and does not touch the free troposphere. In between there is so-called entrainment interface layer, EIL, of thickness varying from few meters to few tens of meters Gerber et al., (2002), Haman et al. (2007), Kurowski et.al., (2009). Data from the majority of field campaigns and numerical simulations are of too poor resolution to infer about details of this layer. In this note we present two cases of very different structures of stratocumulus top, capping inversion and EIL, documented by means of very high spatial resolution measurements of temperature and liquid water content. Analyzed airborne data were collected in course of Physics of Stratocumulus Top (POST) research campaign performed in 2008 Gerber et al. (2010, 2012). The present document is structured in a following way: information of POST and key instruments are in section 2, data from two contrasting cases TO10 and TO13 are described in section 3 and discussed in section 4.

2. POST: PHYSICS OF STRATOCUMULUS TOP RESEARCH CAMPAIGN

Physics of Stratocumulus Top (POST) was a research campaign held in the vicinity of Monterey Bay in July and August 2008. High-resolution in-situ measurements with CIRPAS Twin Otter research aircraft were focused on a detailed study of processes occurring at the interface between the STBL and the free troposphere. The aircraft was equipped to measure thermodynamics, microphysics, dynamics and radiation.

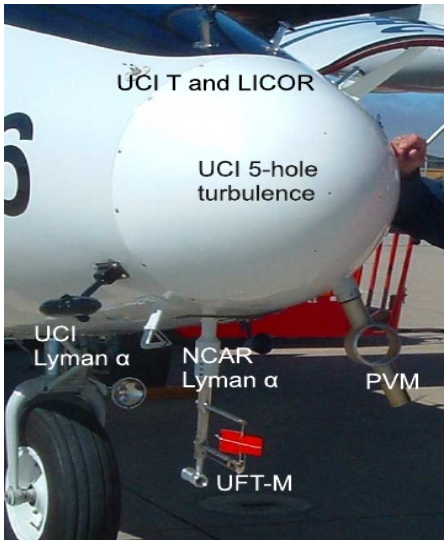

Figure 1. Radome of CRPAS Twin Otter research aircraft with fast-response instruments used in POST.

Adopted flight strategy was aimed at collection of data from the cloud-top region, accompanied by information on fluxes in various levels of STBL and vertical profiles of thermodynamic and dynamic parameters allowing to characterize lower atmosphere

for the purpose of Large Eddy Simulations. Of key interest was cloud top, sampled in course of porpoises across EIL, as shown in Fig.3 of Gerber et al. (2010). In this study we focus on a fine-scale measurements collected with the UFT-M thermometer Kumala et al. (2012), Particulate Volume Monitor PVM-100 Gerber et al. (1994), and other fast-response instruments collocated in close proximity around the radome of the aircraft (Fig.1). The finest resolution PVM and UFT-M data discussed here are of 1000Hz sampling frequency, which corresponds to ~5.5cm spatial resolution at 55m/s true airspeed (TAS) of Twin Otter. Other fast response sensors provided 100Hz and 40Hz (55cm and 1.4m spatial resolution) measurements of three components of turbulent velocity fluctuations and humidity. Data are freely available from the POST database maintained by by National Center of Atmospheric Research Earth Observation Laboratory, http://www.eol.ucar.edu/projects/post/.

Preliminary analysis of collected data performed by Gerber et al. (2010, 2012) allowed to distinguish between ”classical” and ”nonclassical” cases. Out of 17 research flights performed in course of campaign, 6 were characterized as ”classical” and 9 as ”non-classical”. In the following we analyze details of EIL structure in ”classical” TO10 case and ”non-classical” TO13 in order to understand similarities and differences between the cases.

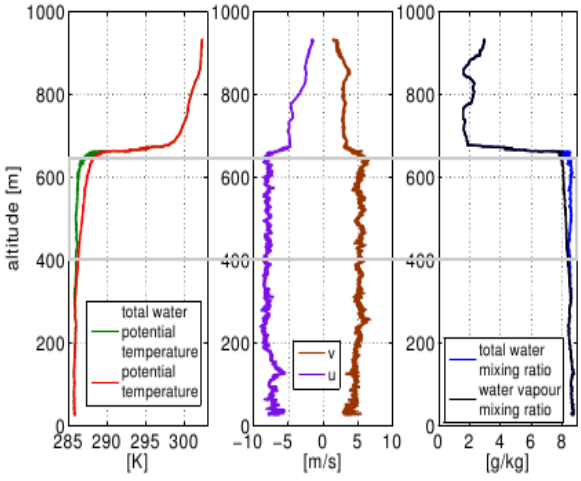

Figure 2. Vertical profiles of potential temperatures,mixing ratios and components of horizontal wind characteristic for TO10 research flight. Cloud layer marked with a gray box.

3. TWO CASES: TO10 AND TO13 FLIGHTS

3.1. CLASSICAL CASE TO10

Flight TO10 was performed on 2008/08/04, 17:15-22:15 UTC. It was a daytime flight (local time was UTC -7h) in a fairly uniform cloud field (c.f. satellite images in POST database). Typical sounding, taken in course of TO10 (Fig.2), shows a sharp liquid water potential temperature θ_l jump (10K) in ~30m thick layer above the cloud top, accompanied by a rapid drop of water vapor mixing ratio and a substantial wind shear (~4m/s for each component of wind velocity).

In Fig.3 records of temperature *T*, liquid water content *LWC*, pressure corrected altitude h, water vapor mixing ratio *r* and fluctuations of three components of velocity (*u,v,w*) in course of typical descend into the cloud deck are presented. Three black vertical lines discriminate between the layers of substantially different properties. The first one, corresponding to the left part of the plot is a free troposphere (FT) above the inversion. Temperature, water vapor mixing ratio and velocity records are smooth, fluctuations are small.

The first black line set at 67726s (659m altitude) marks the end of FT layer. After the marker temperature decreases, fluctuating rapidly. Velocity records show presence of a substantial wind shear and turbulence. Temperature jump of ~8K is recorded in ~13m thick layer on a horizontal distance of ~550m. Such temperature drop, wind shear and turbulence are common features for all porpoises in this flight, suggesting existence of a characteristic Turbulent Inversion Sub-Layer (TISL) above the cloud top. It is worth noticing, that vapor pattern not always mirrors that of *T*. Increased humidity spots, indicating former mixing events (detrainment), are present in FT above TISL.

2nd marker, set at 67736s (644m altitude), indicates entrance into a first blob of a cloud (*LWC*>0). Later aircraft penetrates through a series of cloudy and clear filaments. Inside the last ones a remarkable (amplitude ~2°C) temperature fluctuations are present. Horizontal velocities indicate continuing wind shear, slightly weaker than in TISL. Turbulent velocity fluctuations are increased. Intertwined cloudy and clear air filaments are recorded on a distance of ~800m in ~30m thick layer. This region is named a Cloud Top

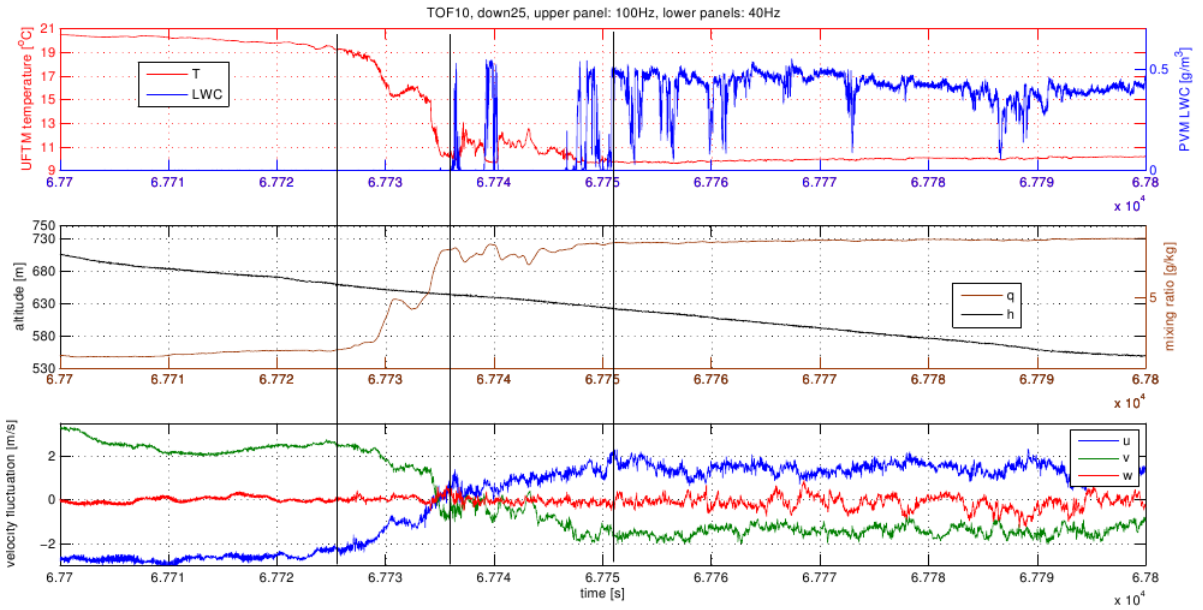

Figure 3. Temperature T, liquid water content LWC, water vapor mixing ratio q and velocity fluctuations (mean value substracted) in course of descend (h-altitude) into the stratocumulus cloud deck. Three black vertical lines mark borders between the free troposphere, the inversion, the cloud mixing layer and the cloud top.

Mixing Sub-Layer (CTMSL). CTMSL together with TISL forms the Entrainment Interface Layer, EIL.

The rightmost black mark at 67751s (628m altitude) indicates entrance into the cloud top layer (CTL). There are remarkable fluctuations of *LWC* inside CTL, but its value at 100Hz (55cm spatial resolution) record is everywhere above 0. Temperature fluctuations are small, typically of 0.2°C, in contrast to that in CTMSL where they exceed 2°C. Velocity fluctuations are still large, especially of a vertical component.

In Fig.4 three expanded segments of 1000Hz *LWC* and *T* records from CTMSL are presented in order to demonstrate character of small-scale *T* and *LWC* fluctuations. It can be seen that locally, in cloudy filaments, *LWC* approaches 0.6gm^{-3} , i.e. the maximum value across the whole cloud depth. These filaments are cold, of temperature ~9.8°C, characteristic for the CTL. Some cloudy filaments with depleted LWC are warmer, of temperatures 10.2-10.6°C. Fluctuations of *LWC* in CTMSL are steeper than fluctuations of *T*. Sometimes (e.g. at 67736.8s) a shift

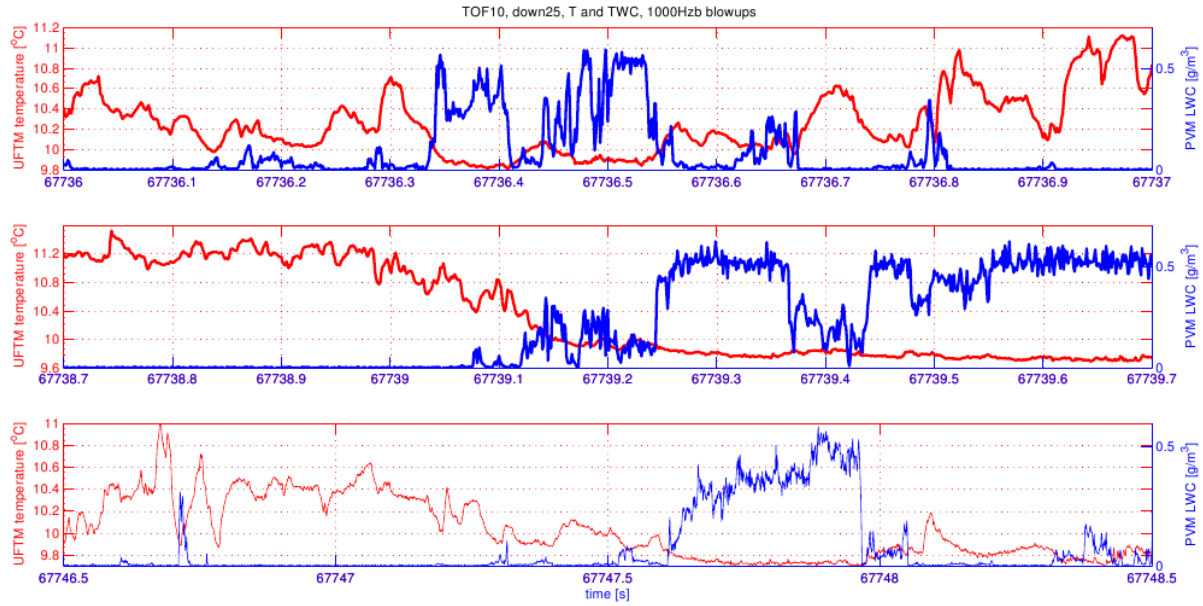

Figure 4. Full 5.5cm resolution (1000Hz) blow-ups of T and LWC fluctuations in the cloud mixing layer. Time corresponds to that in Fig.3. Two upper panels show 1s (55m long) segments, the bottom one shows 2s (110m long) segment.

between *LWC* and *T* peaks can be noticed, most likely effect of different location of PVM and UFT sensors.

Vertical profiles of LWC across CTMSL and CTL from 12 consecutive typical penetrations are presented in Fig.5. Each dot corresponds to LWC averaged over 1.4m long distance (40Hz data). In most subplots the maximum *LWC* increases linearly with height, suggesting presence of parcels lifted (almost) adiabatically from the cloud base, (c.f. Pawlowska et.al., (2000), Gerber (1996)). Parcels with reduced *LWC* most often appear in CTMSL, in CTL depleted *LWC* is less common and indicates presence of ”cloud holes” (Gerber et al. (2005), Kurowski et.al. (2009), Malinowski et al. (2012)), parcels of negative buoyancy, formed in course of mixing and evaporative cooling at the cloud top, slowly descending across the cloud deck.

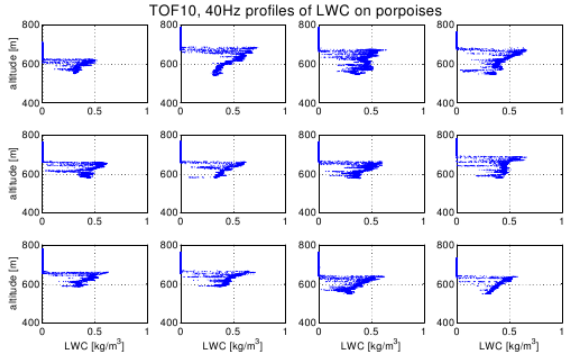

Figure 5. Typical profiles of LWC collected on porpoises in TO10 flight. Each data point corresponds to 1.4m long average (40Hz data). Four consecutive profiles are shown in each row. Successive rows are from different flight legs in order to illustrate LWC profiles for the the whole flight.

3.2. NON-CLASSICAL CASE TO13

Conditions during evening flight TO13, performed 2008/08/09, 00:58-06:00 UTC were different, as illustrated in Fig.6. While the total jump of θ_l between the middle of the mixed layer and the ~1000m altitude is comparable to TO10 case (~10K), a sharp inversion above the cloud top has a temperature jump of no more than ~4K. θ_l and total water profiles are tilted from vertical across the upper part of the cloud. This suggests that the cloud top is not a part of the mixed atmospheric boundary layer.

Humidity profile in Fig.6 shows almost saturated layer (or blob?) at ~750m height. Wind jump in the cloud top region is smaller than in TO10 case and a shear layer is significantly deeper, its bottom correlates with the top of the mixed boundary layer.

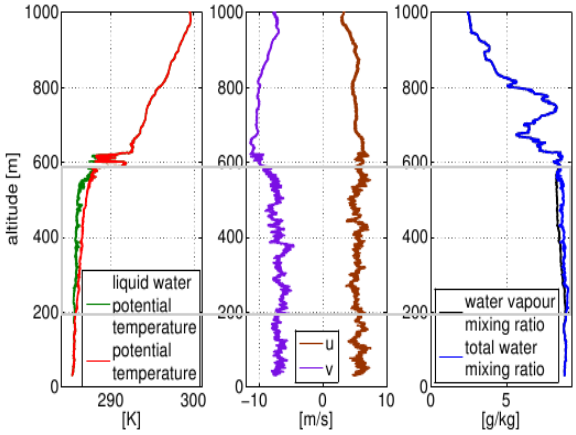

Figure 6. As in Fig.2, but for TO13 flight.

In Fig.7 100Hz series of *T*, *LWC*, *r* and velocity fluctuations in typical penetration of the cloud top are presented. In contrast to TO10 case (c.f. Fig.4), *T, r* and velocity fluctuations are present in FT above EIL. Line discriminating between FT and TISL is set at 14746s (altitude of 599m), marking beginning of the sharp inversion associated with a wind shear (*v* velocity component only). Patterns of *T* and *v* before the marker suggest wavy engulfment of FT air into TISL.

A first blob of cloudy air (14751s, 591m height) marks beginning of CTMSL. There are increased velocity fluctuations associated with this parcel and successive cloud blobs. Later, till 14772s (down to 554m altitude) *T*, *r* and *LWC* vary. Except for the first cloudy filament, *LWC* in CTMSL does not exceed 0.25gm^{-3} , which is substantially less than the maximum *LWC* in cloud top region. This suggests that cloud filaments in this region do not contain adiabatic parcels originating at the cloud base. Humidity in both cloud and clear air filaments approaches the saturation value.

A marker discriminating between CTMSL and CTL is set in a point in which *LWC* jump correlates with drop of *T* and *r*. Right to this point there are remarkable fluctuations of *LWC* and of all velocity components, but no more systematic increase of *v* (end of wind shear layer). Across the whole depth of EIL (between 599m and 554m) temperature changes by less than 2.5K, *v* velocity component changes by ~4m/s and, paradoxically, water vapor mixing ratio

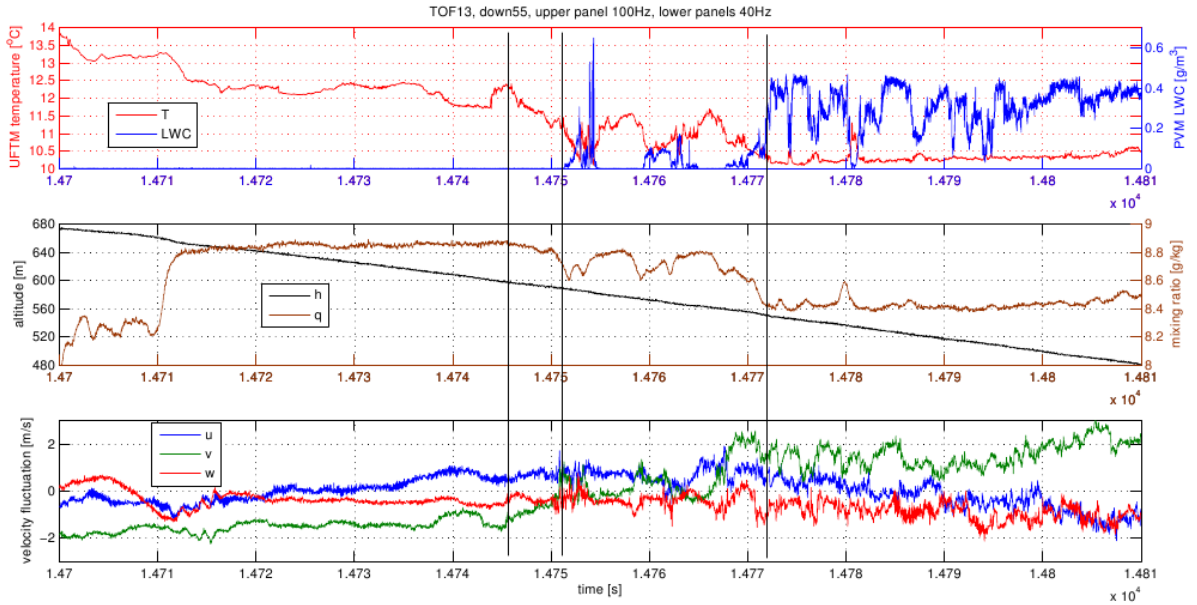

Figure 7. As in Fig.3, but for TO 13 flight.Figure 3.

increases with height, indicating that the whole EIL is close to saturation.

Fig.8 shows 1000Hz blow-ups of *T* and *LWC* fluctuations in CTMSL. Microscale picture of cloud-clear air mixing clearly differs from that in TO10 (c.f. Fig.5). Regions of *LWC*<0.1g/m^3 accompanied by temperature fluctuations of ~0.5K are common. Sharp ramps in temperature record suggest very narrow interfaces between the filaments of various temperatures. Such ramps, common within both: cloudy and clear air filaments were not observed in TO10 case.

In Fig.9 twelve consecutive vertical profiles of LWC in are presented in a similar manner as in Fig.6. Differences between these figures are striking. In TO10 maximum LWC in CTL and CTMSL in 100m thick layer at the cloud top increases with height, in TO13 it decreases or is constant. Several panels indicate that in a layer below 100-150m from the cloud top the maximum LWC shows pattern typical to that in the mixed layer: a linear increase of maximum LWC with the altitude.

It is worth of mentioning, that structure of stratocumulus top in TO13 is not unique. It resembles closely e.g. clod top from RF08B case of FIRE I research campaign (c.f. Fig 6 in Rode and Wang (2007)).

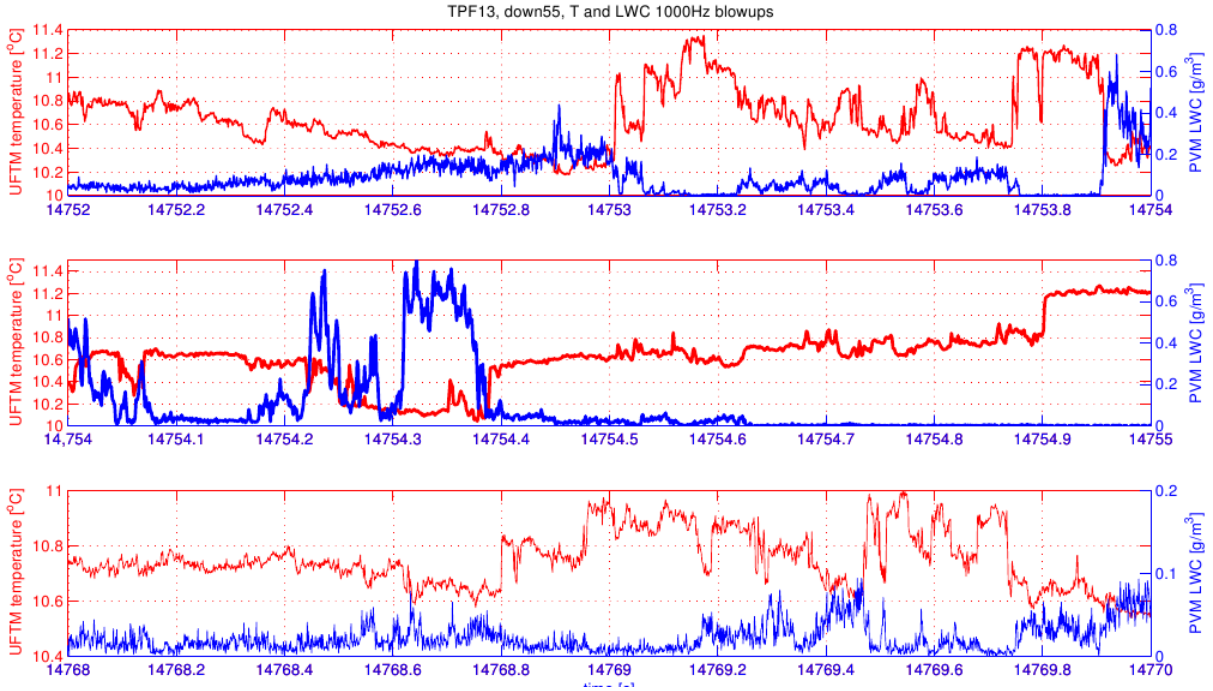

Figure 8. As in Fig.4, but for TO 13 flight. Panels 1 and 3 show 2s (110m long) segments, in the middle panel1s (33m long) segment is presented.

4. DISCUSSION

Differences in thermodynamical and dynamical properties of the cloud tops between TO10 and TO13 cases were reflected in visual appearance of stratocumulus top. Observers on board noticed ”classic stratocumulus layer” in course of TO10 flight, while in course of TO13 they reported ”cloud tops looking like moguls”.

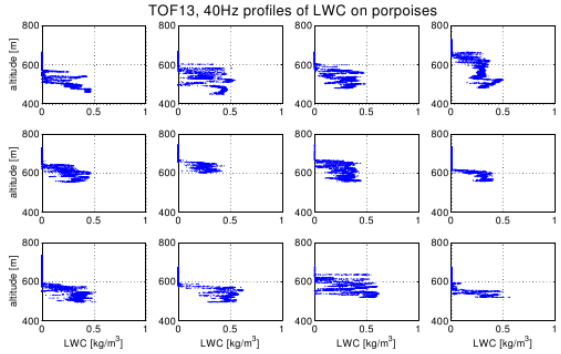

Figure 9. As in Fig.5, but for TO13 flight.

Nature of these differences requires additional analysis. Consider crude estimates of turbulence parameters in consecutive layers and sublayers of the cloud top region (Table 1), based on few penetrations in each case.

TOF10	RMSV	Ri	$\frac{L_C}{L_O}$	TOF13	RMSV	Ri	$\frac{L_C}{L_O}$
FT	0.15	3.9	2.8	FT	0.20	3.9	2.8
TISL	0.49	0.20	0.30	TISL	0.36	0.28	0.38
CTMSL	0.42	0.60	0.68	CTMSL	0.78	0.34	0.44
EIL	0.63	0.39	0.49	EIL	0.72	0.47	0.57
CTL	0.50	-	-	CTL	0.53	-	-

Table 1. Typical properties of turbulence in consecutive layers of the cloud top in TO10 and TO13.

Rows: FT-free troposphere, TISL- turbulent inversion sublayer, CTMSL- cloud top mixing sublayer, CTL- cloud top layer, EIL: entrainment interfacial layer.

Columns: RMSV- root mean square velocity in m/s, Ri- bulk Richardson number, L_C – Corrsin scale, L_O – Ozmidov scale.

Root mean square velocity (RMSV) fluctuations were calculated using low-pass filtered velocity (10Hz cutoff frequency) in order to damp the instrumental noise. Bulk Richardson number was estimated from 1 Hz data across ~50m thick layer of FT, and the whole depths of TISL, CTMSL and EIL using the following formula:

$$Ri = \frac{\frac{g}{\theta_l}\left(\frac{\Delta \theta_l}{\Delta z}\right)}{\left(\frac{\Delta u}{\Delta z}\right)^2 + \left(\frac{\Delta v}{\Delta z}\right)^2} \qquad (1)$$

where g is gravity acceleration, $\Delta\vartheta_l$, Δu and Δv are jumps of liquid water potential temperature and horizontal velocity components across the layer of thickness of Δz.

Vertical gradients are affected by the way data were collected. Almost horizontal flight path (typical inclination 2 degrees) and inevitable horizontal variability of temperature and wind are cause of this problem. In particular, CTMSL as seen in Figs. 3 and 6, may not appear on vertical profiles from. e.g. dropsondes. Thickness of this sublayer is just a ”first guess” estimate of the amplitude of cloud top fluctuations on a horizontal distance of few km.

Keeping above in mind, a simplified dynamical picture of cloud top region in both, such different cases, is surprisingly similar. Free troposphere is dynamically stable (Ri≈4), with the minimum values of RMSV in all the investigated layers. TISL, CTMSL and the whole EIL are characterized by values of Ri close to the critical (which, according to different sources varies in a range 0.2–1.0). Minimum value of Ri seems to be characteristics of TISL. All the penetrations seen by the authors so far confirm that TISL is turbulent, despite the maximum static stability across this layer. SiA border between non-turbulent FT and turbulent TISL is always sharp, no gradual increase of velocity fluctuations is observed. CTL begins at the level where horizontal velocity gradient vanishes. Similar properties of EIL, collected from helicopter-borne instrumented platform ACTOS were reported by Katzwinkel et al., (2011).

Estimates of Ri and RMSV across whole EIL are more reliable than across the sublayers. Despite the uncertainties, turbulent properties of EIL as diagnosed from Ri are similar in both cases. This can be explained analyzing the length scales associated with the turbulence. The first one, Corrsin scale, is a scale above which eddies are deformed by the shear and can be expressed as:

$$L_C = \sqrt{\frac{\epsilon}{S^3}} \qquad (2)$$

In the above S is velocity shear across the EIL and ε is the turbulent kinetic energy dissipation rate. Ozmidov length scale is a scale above which eddies are deformed by a stable stratification in EIL and is expressed as:

$$L_C = \sqrt{\frac{\epsilon}{N^3}} \quad (3)$$

where N is Brunt-Vaisala frequency across the EIL. While we do not know ε in both cases (estimates from the power spectra of velocity on short flight segments are not reliable), we can estimate the ratio of Corrsin and Ozmidov scales:

$$\frac{L_C}{L_O} = \left(\frac{N}{S}\right)^{\frac{3}{2}} = Ri^{\frac{3}{4}} \quad (4)$$

The last equation shows link between the scale ratio and Ri which can be interpreted in a following way: production of turbulence by the shear and across EIL and its damping by the buoyancy across EIL coincides. Ri in range 0.3-0.5 in statically stable turbulent mixing layers is widely reported in the literature (see review by Peltier and Caulfield (2003)), direct numerical simulations of Smyth and Moum (2000) (c.f. Fig 6 therein), of Brucker and Sarkar (2007) (Fig.7 therein) and of Pham and Sarkar (2010) (Fig. 2B therein); consequently show Ri in range 0.3-0.5 in the stratified shear layer in agreement with the laboratory experiments reviewed by Peltier and Caulfield (2003) and with our estimates. More interestingly, Peltier and Caulfield (2003) discuss details of the mechanism which drives mixing across stratified shear layer: overturning of densities in Kelvin-Helmhols billows leading to secondary convective instability across the layer which determine mixing efficiency. What differs Sc cloud top mixing region from stable mixing layers reviewed in the literature is the effect of evaporative cooling in course of mixing, leading to nonlinear effects in buoyancy of mixed parcels. Relative humidity RH of FT in TO10 case is 0.12, while in TO13 it reaches 0.92. In both cases CTL is saturated containing small, typical for stratocumulus clouds, amounts of LWC. Mixing diagram for TO10 case closely resembles that from RF01 of DYCOMS II experiment (c.f. Fig. 11 in Kurowski et.al. (2009)). For dry troposphere parcels containing FT fraction χ<0.12 in mixing event are negatively buoyant, and mixtures of FT fraction χ<0.11 are saturated after completion of mixing. This means, that diluted cloudy parcels of χ<0.12 are likely to be removed from CTML by negative buoyancy.

In contrary, for TO13 case, mixing across inversion cannot produce negative buoyancy. High RH of entrained FT air and small temperature difference between FT and CTL cause that evaporative cooling in course mixing is weak, which only marginally affects buoyancy (density). Additionally, mixtures of as high fraction of clear air as χ<0.7 are still cloudy. In consequence, most of the mixed parcels maintain diluted cloud water and remain close to the level where mixing occurred, which leads to formation of a layer with reduced LWC below the inversion.

5. CONCLUSIONS

1. Inversion capping stratocumulus layer is turbulent.

2. Exchange between FT and CTL is governed by turbulent mixing across EIL. Thickness of EIL results from dynamic adaptation of thickness of the shear layer to temperature (density) and wind jumps between CTL and FT. Adaptation means maintaining the Richardson number close to its critical value.

2. Despite similarities in dynamics of exchange process across EIL, existence or non-existence of cloud top entrainment instability leads to substantial differences of the Sc top structure. When thermodynamic conditions allow CTEI, mixed parcels which are negatively buoyant they are removed from CT region due to negative buoyancy. For high RH of FT, preventing from CTEI, mixed parcels often remain cloudy and buoyancy sorting prevents them from sinking. They remain in the cloud top region below inversion.

Acknowledgments: *This research was supported by the National Science Foundation with the grant ATM-0735121 and by the Polish Ministry of Science and Higher Education with the grant 186/W-POST/2008/0. We thank all POSTers and CIRPAS for the excellent collaboration during the field campaign. The manuscript was written in Kavli Institute for Theoretical Physics at UC Santa Barbara in course of "Nature of Turbulence" program, SPM acknowledges support from KITP.*

References:

Albrecht, B.A., Randall, D.A., Nicholls, S. (1988), Observations of marine stratocumulus clouds during fire,Bull.Amer.Meteor.Soc., 69, 618–626.

Bretherton, C.S., Uttal, T., Fairall, C.W., Yuter, S.E.,Weller, R.A., Baumgardner, D., Comstock, K., Wood. R., Raga, G.B. (2004), The Epic 2001 Stratocumulus Study, Bull.Amer.Meteor.Soc., 85, 967–977.

Brucker, K.A., Sarkar, S. (2007), Evolution of an initially turbulent stratified shear layer, Phys.Fluids, 19, 1050105.

Caughey, S. J.,Crease, B. A., Roach, W. T. (1982), A field study of nocturnal stratocumulus: II. Turbulence structure and entrainment, Q.J.Roy.Meteor.Soc., 108, 125–144.

Faloona, I., Lenschow, D.H, Campos T., Stevens, B., van Zanten, M. (2005), Observations of Entrainment in Eastern Pacific Marine Stratocumulus Using Three Conserved Scalars, J.Atmos.Sci., 62, 3268–3285.

Gerber, H., Arends, B.G., Ackerman, A.S. (1994), A new microphysics sensor for aircraft use, Atmos.Res., 31, 235–252.

Gerber, H. (1996), Microphysics of Marine Stratocumulus Clouds with Two Drizzle Modes, J.Atmos.Sci., 53, 1649–1662.

Gerber , H., S.P. Malinowski, J.-L Brenguier, and F. Burnet (2002): On the entrainment process in stratocumulus clouds. *Proc. 11th Conf. On Cloud Physics*, Ogden, UT, Amer. Meteor. Soc., CD-ROM, paper JP7.6

Gerber, H., Frick, G., Malinowski, S.P., Brenguier, J-L., Burnet, F. (2005), Holes and entrainment in stratocumulus, J.Atmos.Sci., 62, 443–459.

Gerber, H., Frick, G., Malinowski, S.P., Kumala, W., Krueger, S. (2010), POST-A New Look at Stratocumulus, 13th Conference on Cloud Physics, Portland, OR, 2010, American Meteorological Society http://ams.confex.com/ams/pdfpapers/170431.pdf

Gerber, H., Frick, G., Malinowski, S.P, Jonsson H., Khelif D., Krueger S. (2012): Entrainment in Unbroken Stratocumulus. submitted to J.Geophys. Res.

Haman, K.E., Malinowski, S.P., Kurowski, M.J., Gerber, H., Brenguier, J-L. (2007), Small scale mixing processes at the top of a marine stratocumulus - A case study, Q.J.R.Meteorol.Soc., 133, 213–226.

Katzwinkel, J., H. Siebert, and R. A. Shaw. (2011), Observation of a self-limiting, shear-induced turbulent inversion layer above marine stratocumulus. Boundary-Lay. (13p) Meteorol., DOI: 10.1007/s10546-011-9683-4

Kumala, W., Haman, K.E., Kopec, M.K., Malinowski, S.P. (2012), Ultrafast Thermometer UFT-M: High Resolution Temperature Measurements During Physics of Stratocumulus Top (POST), in preparation to Atmos Meas.Tech.

Kurowski, M.J., Malinowski, S.P., Grabowski, W.W. (2009), A numerical investigation of entrainment and transport within a stratocumulus-topped boundary layer, Q.J.R.Meteorol.Soc., 135, 77–92.

Lenschow, D. H., Paluch, I.R., Brandy, A.R, Pearson, R., Kawa S.R, Weaver C.J., Kay, J.G, Thornton D.C., Driedger A.R., (1988), Dynamics and Chemistry of Marine Stratocumulus (DYCOMS) Experiment, Bull.Amer.Meteor.Soc., 69, 1058–1067.

Lenschow, D.L., Zhou, M., Zeng, X., Chen, L., Xu, X., (2000), Measurements of fine-scale structure at the top of marine stratocumulus, Boundary Layer Meteorol., 97, 331–357.

Lilly, D. K. (1968) Models of cloud-topped mixed layers under a strong inversion, Q.J.R.Meteorol.Soc., 94, 292–309.

Lilly, D. K. (2008), Validation of a mixed-layer closure. II: Observational tests, Q.J.R.Meteorol.Soc., 134, 57–67.

Malinowski, S.P., Haman, K.E, Kopec M.K., Kumala, W., Gerber H.E., Krueger, S.K (2010),Small scale variability of temperature and LWC at Stratocumulus top , 13th Conference on Cloud Physics, Portland, OR, 2010, American Meteorological Society http://ams.confex.com/ams/pdfpapers/171260.pdf

Moeng C-H., Stevens B., Sullivan PP. (2005), Where is the interface of the stratocumulus-topped PBL?, J. Atmos. Sci., 62, 2626–2631.

Nicholls, S. (1989), The structure of radiatively driven convection in stratocumulus, Q.J.R.Meteorol.Soc., 115, 487–511.

Pawlowska, H., Brenguier, J-L., Burnet, F. (2000), Microphysical properties of

stratocumulus clouds, Atmos.Res., 55, 15–23.

Peltier, W.R., Caulfield C.P. (2003), Mixing Efficiency in stratified shear flows.Annu.Rev.Fluid.Mech., 35, 135–167.

Pham, H.T., Sarkar, S. (2010), Transport and mixing of density in a continuously stratified shear layer.J.of.Turbulence, 11, 1–23.

Roode, S.R., Wang, Q. (2007), Do stratocumulus clouds detrain? FIRE I data revisited, Boundary-Layer Meteorol., 122, 479–491.

Smyth, W.D., Moum, J.N. (2000), Length scales of turbulence in stably stratified mixing layers, Phys.Fluids, 12, 1327–1342.

Sorbjan, Z. (2010), Gradient-based scales and similarity laws in the stable boundary layer, Q.J.R.Meteorol.Soc., 136, 1243–1254.

Stevens, B. (2002), Entrainment in stratocumulus-topped mixed layers, Q.J.R.Meteorol.Soc., 128, 2663-2690.

Stevens, B., Lenschow, D.H., Vali, G., Gerber, H., Bandy, A., Blomquist, B., Brenguier, J-L., Bretherton, C. S., Burnet, F., Campos, T., Chai, S., Faloona, I., Friesen, D., Haimov, S., Laursen, K., Lilly, D.K., Loehrer, S.M., Malinowski, S.P., Morley, B., Petters, M.D., Rogers, D.C., Russell, L., SavicJovcic, V., Snider, J.R., Straub, D., Szumowski, M.J., Takagi, H., Thornton, D.C., Tschudi, M., Twohy, C., Wetzel, M., van Zanten, M.C. (2003), Dynamics and chemistry of marine stratocumulus - Dycoms II, Bull. Amer. Meteorol.Soc., 84, 579–593.

Stevens B., Moeng C.H., Ackerman A.S., Bretherton C.S., Chlond A., De Roode S., Edwards J., Golaz J.C., Jiang H.L., Khairoutdinov M., Kirkpatrick M.P., Lewellen D.C., Lock A., Muller F., Stevens D.E., Whelan E., Zhu P. (2005), Evaluation of large-Eddy simulations via observations of nocturnal marine stratocumulus, Mon. Wea. Rev., 133, 1443–1462.

Wang, S., Golaz, J.-C., Wang, Q. (2008), Efect of intense wind shear across the inversion on stratocumulus clouds, Geophys.Res.Lett., 35, L15814.

Yamaguchi, T., Randall, D.A., (2008), Large-Eddy Simulation of Evaporatively Driven Entrainment in Cloud-Topped Mixed Layers, J. Atmos. Sci., 65, 1481–1504.

Yamaguchi, T., Randall, D.A., (2012), Cooling of entrained parcels in a large-eddy simulation. J.Atmos. Sci., 69, 1118-1136.